Journal of Materials Chemistry C

RSC Publishing

PAPER

View Article Online
View Journal

Cite this: DOI: 10.1039/c3tc30679h

Competition between morphological attributes in the thermal annealing and additive processing of polymer solar cells†

Wei Ma,[a] Long Ye,[bc] Shaoqing Zhang,[b] Jianhui Hou*[b] and Harald Ade*[a]

Received 12th April 2013
Accepted 27th June 2013

DOI: 10.1039/c3tc30679h

www.rsc.org/MaterialsC

Thermal annealing and additive processing are employed and compared using alkoxy substituted (QxO) and extended π conjugated alkythienyl substituted (QxT) benzo[1,2-*b*:4,5 *b*′]dithiophene based heterojunction (BHJ) solar cells. The characteristic median length of the morphology, average composition fluctuations, interface structure, crystallinity and molecular miscibility are investigated based on these two processes. Our results suggest that focusing on single structural, morphological or thermodynamic measurements is not sufficient to explain differences in device performance. In the current work, no blends are close to the ideal morphology containing either domains that are too large, too mixed or too pure. An optimization strategy is proposed to improve those devices. Importantly, we find that domain size and relative domain purity are overall correlated with molecular miscibility, *i.e.* the more immiscible system induces larger and purer domains irrespective of the processing and even in non-equilibrium structures. This indicates that the relative domain size and purity, and device performance can be potentially predicted by the donor–acceptor molecular miscibility, a factor not yet widely considered when designing new materials for BHJ devices.

1 Introduction

Solar cells based on polymer : fullerene, donor : acceptor bulk-heterojunctions (BHJ) have attracted increasing interest for next generation solar cell conversion technologies due to the potential for low cost and scalable processing from solutions.[1–3] Significant progress in device performance has been made as evidenced by the improvement in the last fifteen years in power conversion efficiencies (PCE) from 1% to 9%.[4,5] This progress has been primarily achieved through heuristic approaches, where new materials are developed following mostly intuition and synthesis along structural motifs that include donor–acceptor/push–pull alternating backbones,[6,7] substitutions,[8–12] and extended π chain side chains,[13–15] *etc.* Synthesis is subsequently followed by a trial-and-error approach to devices optimization. The parameters that are modified in order to manipulate the device morphology and thus performance include donor : acceptor ratio,[16,17] molecular weight,[18] choice of solvent,[19–22] thermal annealing,[7] solvent annealing,[23] and increasingly the use of solvent mixtures and additives.[22,24] Systematic guidance either by theory/modelling or knowledge of fundamental interactions and thermodynamic properties is currently lacking even though it would be universally beneficial for rational molecular design. Following the observation that fullerenes are miscible in the amorphous regions of P3HT and many other polymers,[25–28] efforts are underway to use miscibility as one predictive parameter to device performance and optimization strategies.[7,29] Here, we delineate that relatively small changes in molecular structure causes numerous device parameters such as the characteristic median length scale of the morphology (for simply also referred as domain size), average composition fluctuation (for simplicity also referred to as relative domain purity), molecular ordering relative to the heterojunction interface, and molecular miscibility to change simultaneously, thus exemplifying and compounding the difficulty to predict performance through knowledge-guided molecular design. At the same time, we show that measurements of fullerene miscibility and the effects of the very common processing aid 1,8-diiodooctane (DIO) provide guidance to improve at least the device processing strategy. Specifically, we show that molecular miscibility can be used to predict the relative domain size and domain purity, which are two important morphological parameters that impact device performance.

In this work, we systematically investigate the domain size and relative purity, crystalline structure, molecular orientation, and thermodynamic properties of alkoxy substituted

[a]*Department of Physics, North Carolina State University, Raleigh, North Carolina 27695, USA. E-mail: harald_ade@ncsu.edu*

[b]*State Key Laboratory of Polymer Physics and Chemistry, Beijing National Laboratory for Molecular Sciences, Institute of Chemistry, Chinese Academy of Sciences, Beijing 100190, China. E-mail: hjhzlz@iccas.ac.cn*

[c]*Graduate University of Chinese Academy of Sciences, Beijing 100049, China*

† Electronic supplementary information (ESI) available. See DOI: 10.1039/c3tc30679h

benzo-[1,2-*b*:4,5-*b*′]dithiophene (PBDTDTQx-O, or QxO for short) and extended π conjugated alkythienyl substituted (PBDTDTQx-T, or QxT for short) based BHJ solar cells as shown in Scheme 1, blended with $PC_{71}BM$ as the active layer. These materials have a dominant absorption peak at 600 nm with an onset near 700 nm.[30] They are thus not expected to yield record efficiencies, but are useful materials to explore the impact of structural themes, such as conjugated side-chains, on morphology and performance. Utilizing the enhanced contrast and easy access to the low-q range of resonant soft X-ray scattering (R-SoXS)[31–33] the domain size and relative purity between polymer-rich and fullerene-rich phases were obtained. Molecular orientation relative to the donor–acceptor interface can be revealed by polarized soft X-ray scattering (P-SoXS).[7,34] Finally, we measure the miscibility[27,28] of $PC_{71}BM$ with QxO and QxT by near edge X-ray absorption fine structure (NEXAFS) spectroscopy and the crystalline structure as determined with grazing incidence wide angle X-ray scattering (GI-WAXS). These measurements result in a comprehensive picture of the structure and morphology that are then linked with device performance for QxO- and QxT-based devices. Overall, we demonstrate that focusing on a single structural, morphological, or thermodynamic measurement is not sufficient to explain the performance changes in these BHJ solar cells. Replacing alkoxy substituted BDT unit with extending π conjugated alkythienyl substitution to make QxT-based polymers alters the domain size, domain purity and molecular miscibility, and less pronounced the crystallinity and interface structure. We note that the observed fullerene miscibility in QxO is only ~5% and thus one of the lowest miscibility levels observed to date.[7,27,28,35–39] Other polymers with low miscibility have shown great performance,[7,39] thus indicating that the potential of QxO might not have been realized.

The chemical structure changes might furthermore impact the morphological response to processing additives. Use of processing additives has been previously shown as an effective method to improve photovoltaic performance in some cases.[40–42] It has been demonstrated that this improvement is achieved by creating a favorable morphology.[22,35,43] In many cases, when 1–8% (volume fraction) of additive is employed, the enhancement of performance can be dramatic. In addition, the performance and implied morphology can be extremely sensitive to the amount of additive. For example, the morphology and performance of small molecular 5,5′-bis{(4-(7-hexylthiophen-2-yl) thiophen-2-yl)-[1,2,5]thiadiazolo[3,4-c]pyridine}-3,3′-di-2-ethylhexylsilylene-2,2′-bithiophene, $DTS(PTTh_2)_2$ processed with 0.25% and 0.6% DIO are significantly different.[41] This sensitivity is shown to be also highly materials dependent.[42] For example, DIO is widely used to enhance performance for a large range of polymers, but is unsuccessful at improving the performance of P3HT based devices.[20] In general and although the importance of mixed domains is activity investigated,[7,38,44,45] the combined evidence suggests that small and pure domains,[7,10,22] sharp interface,[22,46] "face-on" orientation relative to electrodes[47,48] and to the D/A interface[7,49] will benefit device performance. These attributes remain the general goal of morphology optimization. Only if the domains are too large or form isolated islands is mixing beneficial to charge generation and needed to provide charge transport pathways for charge carriers.[7,38] Generally, achieving an optimized morphology where each parameter is optimized is very difficult and the process to do so is likely materials dependent. The competition of those parameters will determine the processing route to optimized performance for a given material. In case of using a processing additive, selecting the nature and amount of additive will be critical to control domain size, composition fluctuations/purity, interface roughness and molecular orientation. The final device performance is governed by the compounded impact of those structural parameters and often only a compromise is achieved in actual devices.[7,21,23,42] Our results indicate that neither the QxO nor the QxT systems have yet been optimized with common fabrication procedure. Our measurements thus provide guidance for the synthesis as well as improved processing, results that provide also guidance on how to optimize other materials systems.

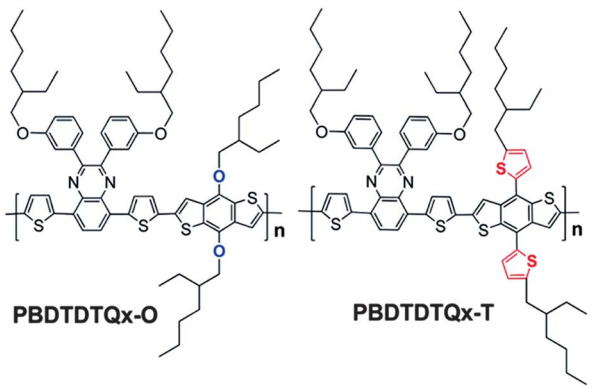

Scheme 1 Chemical structures of polymer PBDTDTQx-O and PBDTDTQx-T.

2 Results

2.1 Device performance

Solar cells were fabricated by spin-coating polymers, QxO and QxT, mixed with $PC_{71}BM$ in 1 : 2 w/w ratio solution in 1,2-dichlorobenzene (DCB) onto pre-coated ITO/PEDOT:PSS layers. The thickness of QxO and QxT based films are ~125 nm and ~80 nm. The substrates were subsequently annealed at 120 °C for 10 min, followed by vacuum evaporation of LiF/Al (1 nm/80 nm) metal electrodes. Current density *vs.* voltage (*J*–*V*) curves are shown in Fig. 1, with the photovoltaic characteristics summarized in Table 1. Nearly identical device performance to Duan *et al.* was achieved, with PCE = 5.17% for devices for QxT:$PC_{71}BM$ (called QxT-annealed for short) with J_{sc} = 11.35 mA cm^{-2}, V_{oc} = 0.76 V, FF = 0.60.[30] As a comparison, QxO:$PC_{71}BM$ (called QxO-annealed for short) shows lower J_{sc} = 7.16 mA cm^{-2}, lower V_{oc} = 0.73 V and identical FF = 0.60. It is reported in Duan *et al.* that the thinner QxT based films exhibit naturally lower UV absorption between 350 and 700 nm while the External Quantum Efficiency (EQE) is higher than for the thicker QxO based films (see ESI, Fig. S1†).[30] This strongly indicates that QxT based films must possess a favorable morphology. When 3% DIO is employed as processing solvent (without additional thermal annealing), no improvement is

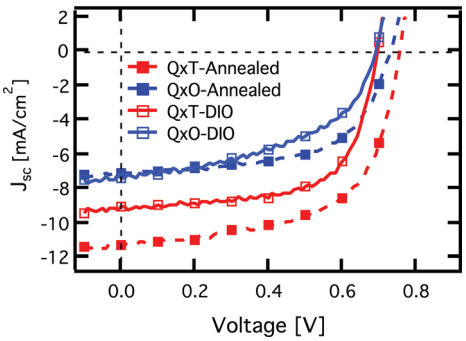

Fig. 1 Device performance based on annealed QxO, QxT blend films, and QxO and QxT processed with DIO.

observed compared to annealing. The PCE of QxO-DIO, QxO-annealed, QxT-DIO and QxT-annealed is 2.49%, 3.10%, 4.20%, and 5.17%, respectively (results shown in Table 1 and Fig. 1). The differences in device performance depending on the use of QxO *vs.* QxT are dramatic. Furthermore, additive processing leads to lower efficiency for both polymers, but thermal annealing and additive processing affects the individual photovoltaic parameters (J_{sc}, V_{oc}, FF) in different ways. It is presumed that these differences are at least in part due to morphological variations since the chemical structure of the conjugated polymers is not exceedingly different and the basic photophysics should be similar.

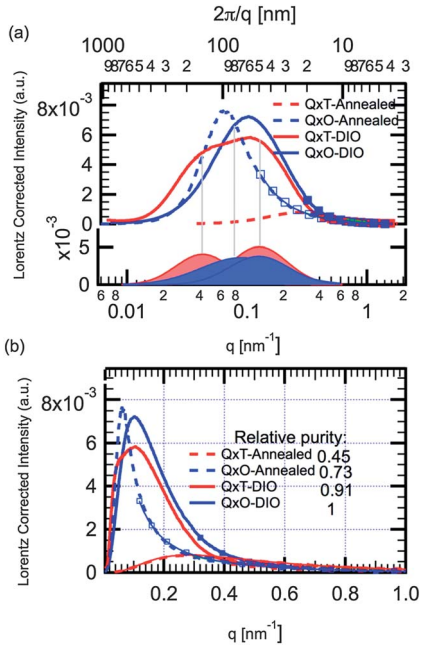

Fig. 2 Azimuthally integrated R-SoXS scattering intensity of blend films QxO:$PC_{71}BM$ and QxT:$PC_{71}BM$ acquired with photon energy of 284.2 eV. (a) lin–log plot, which readily shows the log-normal distributions of the spatial frequencies that characterize the sample morphology, Bottom shows log-normal fits of the scattering profiles for the QxO-DIO and QxT-DIO samples. (b) lin–lin plot of the scattering, the natural representation to visually judge the total scattering intensity that reveals the composition fluctuations. From the total scattering (the area under the graphs), the relative domain purities are deduced as indicated.

2.2 Domain size and purity

Resonant soft X-ray scattering (R-SoXS) was utilized to probe the median characteristic length scales of the morphology and the average composition fluctuations, *i.e.* the relative purity between polymer-rich and fullerene-rich domains within a two phase model that is appropriate here due to the low crystallinity of the materials (see below).[19,22,30,32–35] A photon energy of 284.2 eV was selected to provide high polymer : fullerene contrast while avoiding high absorption in the resonant peaks and above the absorption edges which can lead to beam damage[50] and background fluorescence. (The contrast functions of polymer : fullerene, polymer : vacuum and fullerene:vacuum near the carbon 1s absorption edge are displayed in Fig. S2.†) Fig. 2 shows the scattering profiles acquired at 284.2 eV for QxO and QxT-based blend films with $PC_{71}BM$ annealed at 120 °C for 10 min and blend thin films cast with 3% DIO. The scattering profiles represent the distribution function of spatial frequency, s ($s = q/2\pi$), of the samples and are dominated by log-normal distributions that can be fitted by a set of Gaussians in lin-log space (shown at the bottom of Fig. 2(a) for QxO-DIO and QxT-DIO samples and supporting information Fig. S3† for all the samples). The median of the distribution s_{median} corresponds to the characteristic median length scale, ξ, of the corresponding log-normal distribution in real space with $\xi = 1/s_{median}$, a model independent statistical quantity. Within a simple morphological model, this would correspond to the median domain spacing and the median domain size would be roughly $\xi/2$. ξ ~86 nm and ~18 nm was observed for QxO and QxT blends with thermal annealing, respectively. When 3% DIO is employed for QxT blend film, ξ is dramatically enlarged. A broad special frequency distribution is observed. This distribution is then fitted with two log-normal functions and reveals ξ of 38 nm and 108 nm, respectively. When QxO blend film is processed with 3% DIO, the morphology shows also two distributions with ξ at 36 nm and 40 nm, slightly reduced compared to QxO-annealed.

Table 1 Photovoltaic data and summary of structural characterization of QxO and QxT-based polymer blends with $PC_{71}BM$ annealed or as-cast with 3% DIO

Active layer	Thickness (nm)	J_{sc} (mA cm^{-2})	V_{oc} (V)	FF	PCE (%)	Miscibility	ξ (nm)	Relative purity	Anisotropy	Scaling
QxO:$PC_{71}BM$-annealed	~125	7.16 ± 0.09	0.73 ± 0.01	0.60 ± 0.03	3.10 ± 0.10	0.05 ± 0.01	86	0.73	0.21	−3.75
QxO:$PC_{71}BM$-DIO	~125	7.41 ± 0.06	0.69 ± 0.01	0.53 ± 0.02	2.49 ± 0.10	0.05 ± 0.01	36 + 40	1	0.16	NA
QxT:$PC_{71}BM$-annealed	~80	11.35 ± 0.07	0.76 ± 0.01	0.60 ± 0.02	5.17 ± 0.10	0.11 ± 0.01	18	0.45	0.18	NA
QxT:$PC_{71}BM$-DIO	~80	9.14 ± 0.07	0.70 ± 0.01	0.65 ± 0.02	4.20 ± 0.10	0.11 ± 0.01	38 + 108	0.91	0.17	−3.74

Within a two phase model, the relative domain purity of the domains, averaged over the size-scale probed, can be extracted by calculating the total scattering intensity (TSI) by integrating the scattering profiles.[22,35] As the q range for QxT-annealed is limited and does not capture the complete domain size distribution, the TSI for this sample is calculated by extending the q range with a log-normal distribution. The TSI reflects the average composition fluctuations, a statistical measure that is model independent. For simplicity, and because of the low crystallinity of the devices, we utilize the two phase model as framework. Relative domain purities of 0.73 ± 0.05, 0.45 ± 0.03, to 0.91 ± 0.02 were obtained for QxO-annealed, QxT-annealed, and QxT-DIO, respectively, with the purity of QxO-DIO being set to 1 as a reference. Details, error determination, and a complementary analysis method are detailed in the supporting information. We note that the difference in terms of domain purity is not originating from crystallinity since both of these polymers show similar amorphous nature as characterized by GIWAXS (shown in ESI, Fig. S4†). In both thermally annealed and DIO processed samples, higher relative domain purity values of QxO-based blend films imply that the QxT-based devices have relatively mixed domains compared to QxO devices.

2.3 Molecular miscibility and spinodal decomposition

The molecular miscibility between fullerene and the donor polymer reflects the basic thermodynamic properties of donor and acceptor, in turn reflecting the driving force for mixing or phase separation between donor and acceptor materials. The resulting complex morphology and level of purity of mixed domains impacts exciton diffusion and charge separation/transport processes in BHJ organic solar cell as discussed above.[27,28] The TSI for QxT-based blends indicates that domain purity is lower compared to that with QxO for both thermal annealing and additive processing. This implies that the driving force for phase separation is lower and hence that molecular miscibility of fullerene in the polymer is higher for solar cells based on QxT. To confirm this point, following previously established methodologies,[51] NEXAFS spectra were acquired of the molecularly mixed regions of films that had been thermally annealed aggressively to yield large domains at a composition equilibrium. The initial blend ratios (polymer : fullerene by weight) were 1 : 2 for QxO and QxT-based blends. Blend films were annealed in a N_2 filled glove box at 180 °C for 96 h to yield complete phase separation. The PCBM formed large domains as observed by visible light microscopy and Scanning Transmission X-ray Microscopy (STXM) (see Fig. 3). NEXAFS spectra (270 to 400 eV) were acquired between the large PCBM domains (see Fig. 4). These NEXAFS spectra were fitted using pure component references for the respective polymer and fullerene.[27,28,51] The resulting fullerene miscibility with QxO is 5.5(8)% (fullerene weight percentage) for $PC_{71}BM$. Relative moderate $PC_{71}BM$ miscibility of 11.5(8)% in relation to prior miscibility measurements[27,28,37,51] were extracted for QxT-based blend films, which is nonetheless about twice as high as that observed for QxT.

Phase separation mechanism of organic materials blends has been studied intensively.[23,40,52–54] In the OPV field, crystallization[55] and spinodal decomposition[56] have been proposed as the driving force of phase separation for polymer/fullerene blends. For the most widely investigated organic solar cells P3HT/PCBM, it is generally considered that crystallization drives phase separation of P3HT and PCBM as P3HT is a highly-crystalline polymer.[55,57] The phase separation mechanism of more amorphous polymers (such as QxO and QxT) and PCBM has not yet been studied intensively. A quasi-bicontinuous

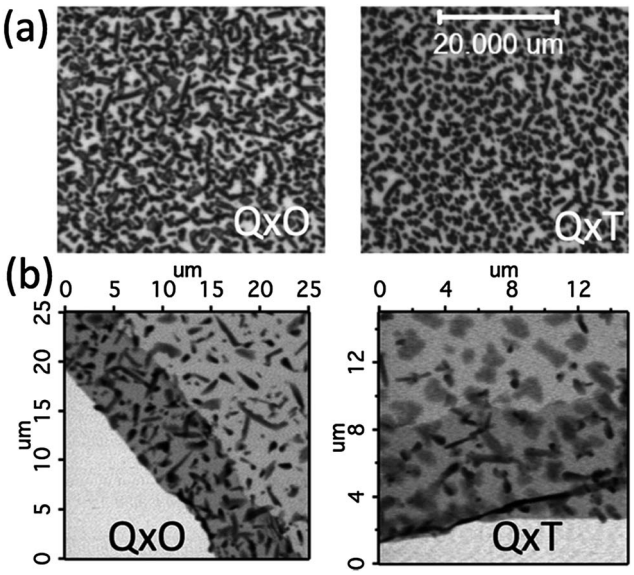

Fig. 3 (a) Visible light microscopy images and (b) Scanning Transmission X-ray Microscopy (STXM) of QxO and QxT after 96 h thermal annealing at 180 °C.

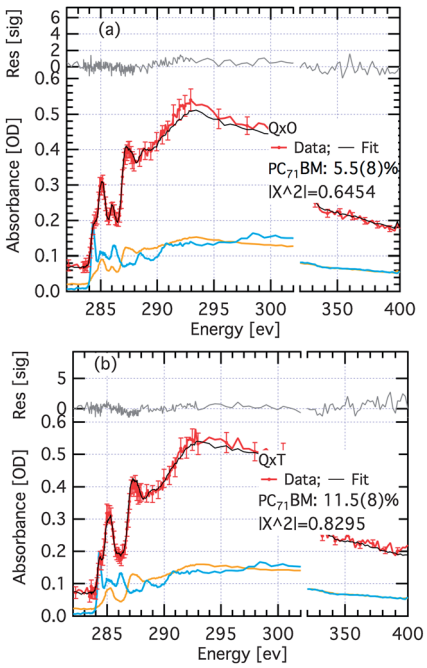

Fig. 4 Fitted NEXAFS spectra of the mixed polymer : fullerene matrix between PCBM agglomerates after annealing polymer : fullerene blend films for 96 h at 180 °C: (a) QxO:$PC_{71}BM$; (b) QxT:$PC_{71}BM$. Yellow and blue curves are from polymer and fullerene reference films.

morphology is observed for both QxO and QxT based blends (see Fig. 3). A bicontinuous structure at this length scale could not be achieved with a semi-crystalline polymer such as P3HT where often needles are observed[58,59] and is also in stark contrast to the round domains observed in PTB7.[35] The quasi bi-continuous structure indicates that the phase separation of QxO and QxT based blends are likely driven by spinodal decomposition, enabled by the relatively low miscibility and low crystallinity. We note that these samples were prepared for the miscibility measurements. The conditions used for the miscibility measurements are extreme and the bi-continuous structure has significantly coarsened and is already breaking up and transitioning to form dispersions. Nonetheless, bicontinuous structures do not emerge from dispersions, so the less aggressive annealing used for device fabrication is likely also leading to bi-continuous morphologies.

2.4 Interface structure and molecular orientation relative to D/A interface

It has recently been reported that molecular orientation relative to the donor–acceptor interface revealed by scattering anisotropy could be an important parameter that impacts charge transport and exciton dissociation and consequently polymer/fullerene organic solar cell device performance.[7] This suggestion is also supported by polymer/polymer and small molecular bilayer organic solar cells.[34,49] Interestingly, strong scattering anisotropy as shown in Fig. 5(a) is observed for all samples. The intensity difference between perpendicular and parallel sectors signifies the degree of molecular orientation, *i.e.* only identical perpendicular and parallel scattering intensity corresponds to random orientation. We note that the scattering profiles shown in Fig. 5(b) are more intense when the sector is perpendicular to the electric field than parallel to the electric field. This suggests a preferential "face-on" polymer orientation relative to the polymer/fullerene interface.[7,34] Such orientation has been shown in small molecule model systems to promote efficient exciton dissociation and prevent charge recombination.[34,49] In order to compare the molecular orientation quantitatively, anisotropy is defined here as the difference of total sector scattering intensity (SSI) in perpendicular and parallel directions over the respective sum $(SSI_{perp.} - SSI_{parall.})/(SSI_{perp.} + SSI_{parall.})$. Values of 0.21, 0.18, 0.16 and 0.17 are obtained for QxO-annealed, QxT-annealed, QxO-DIO and QxT-DIO blend films, respectively. (The SSI of QxO is obtained by fitting a log-normal function.) This indicates that the degree of molecular orientation in the devices is rather similar. When DIO is employed, in-plane molecular ordering is slightly reduced for both polymers. We note that for QxT-DIO blends, only the high-q peak shows anisotropy. Further modeling needs to be developed to better understand this phenomenon in detail and its effect on performance. In this particular instance, the similar results suggest that in-plane molecular orientational correlations do not preferentially impact the devices performance.

As mentioned before, most scattering profiles can be fitted very well by one or two log-normal functions. In some cases, the high-q data cannot be fitted well with such an approach alone and the high-q scattering was fitted with a Porod scaling exponent function.[22,35] A scaling exponent of -4 indicates a sharp interface while smaller or bigger exponent than -4 implies diffuse or fractal rough interfaces, respectively. The fitted scaling exponents are shown in ESI, Fig. S3,† where scaling exponents of QxT-DIO and QxT-annealing can be obtained, yielding very similar values of -3.74 and -3.75, respectively, in the q range available. This indicates slightly rough interfaces. Due to the limitation of q-range, heterojunction interface structure cannot be measured for QxO/DIO and QxO/annealed blends, preventing a comparison of this aspect between systems.

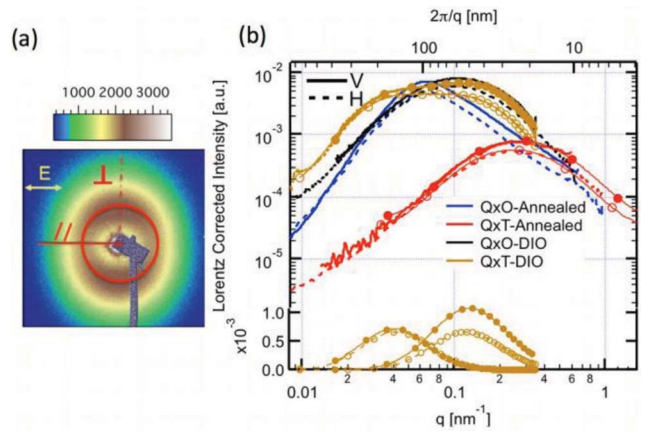

Fig. 5 (a) 2D scattering pattern at 284.2 eV for QxO-annealed. (b) P-SoXS scattering profiles of polymer:$PC_{71}BM$ blend films: QxO-annealed, QxO-annealed thermally annealed as indicated; QxT-DIO and QxT-DIO. Solid lines/solid circles and dash lines/open circles represent data average over 10° azimuthal sectors perpendicular and parallel to the photon polarization, respectively. The bottom part of the figure shows the corresponding log-normal contributions.

3 Discussion and conclusions

The effect of using thermal annealing or processing additive as the optimation tool depends strongly on the material. Annealing improves V_{oc} over the use of DIO, presumably from favorable surface/interface segregation, a morphological aspect which we did not explicitly verify due to the relatively small impact of V_{oc} on the overall performance differences. Other possible factors influencing V_{oc}, such as HOMO–LUMO shifts due to changes in ordering or differences in relative orientations at the interface can be ruled out due to the measured similar crystallization and scattering anisotropy. Much of the relation of morphology to J_{sc} can be readily understood using the classical device paradigm. The smallest ξ, *i.e.* 18 nm for QxT-annealed, leads to the largest J_{sc} and the largest ξ, *i.e.* 86 nm for QxQ-annealed, leads to the lowest J_{sc}, an effect that would be even more pronounced when considering the higher absorption of the thicker QxO films. The J_{sc} improves somewhat for QxO with the use of DIO as the additive causes smaller domains than annealing. The reverse but consistent observation is made for OxT, where the use of DIO increases the domains and the J_{sc} drops. The overall ranking of QxO-DIO, which has on average slightly smaller and more pure domains than QxT-DIO, yet a lower J_{sc}, does not seem to fit this pattern. We note though that

the J_{sc} of QxO-DIO is negatively impacted by a low FF and that if a stronger reverse field would be applied the current is expected to increase relative to QxT-DIO and be more in-line with the measured domain size. We will discuss this further below, after having considered the relation of FF to morphology.

Overall, there is no strong monotonic relation of FF to any of the device characteristics measured, an analysis that might also be complicated by the difference in thicknesses between devices. Overall, this is not surprising, In general, FF can depend on several complex processes, including field dependent geminate recombination and charge separation, and bimolecular recombination, and a number of morphological aspects. Regarding morphology, FF is negatively impacted if domains or too impure[7,35,60] and can be negatively impacted by isolated charge traps if the domains are too pure.[7,38] A detailed characterization of these factors was outside the scope of the present study. The lowest FF was observed for QxO-DIO, despite this being the devices with the largest composition fluctuations. We note here that two recent studies have argued that a threshold level of minority species is required in mixed domains in order to provide percolation pathways for the charges.[7,38] Bartlet *et al.* in particular concluded that the fullerene concentration in mixed domains can become too low, leading to isolated fullerene molecules which become electron traps that enhance charge recombination, which in turn negatively impacts FF. We suggest that a similar mechanism might contribute to the poor performance of QxO-DIO, exaggerated by the thicker films of the QxO devices. The use of DIO and largely amorphous polymers tends to lead to round, nearly pure $PC_{71}BM$ domains.[35] If indeed the domains observed for QxO-DIO with a relatively small ξ of 36 nm are nearly pure $PC_{71}BM$ domains dispersed in a much thicker film, then the transport of electrons through the polymer *via* the percolation pathways provided by the $PC_{71}BM$ in mixed polymer : fullerene domain is critical. These results contrast with those for high performance PTB7, which has a fullerene miscibility of ~30% and thus a concentration of PCBM in the mixed domains above the percolation threshold.[35] The low fullerene concentration in QxO-DIO thus leads primarily to a reduced fill factor and only indirectly contributes to the reduced J_{sc} with respect to QxT-DIO. As charges would be swept out more effectively with a larger reverse bias, the *J–V* graphs suggest that the current for QxO-DIO might actually exceed that for QxT-DIO at significant reverse bias. The best FF of 0.65 has been observed for intermediate purity, with higher impurity leading to a moderate drop in FF.

Relating miscibility to morphology, we note that for both thermal annealing and additive processing, QxO-based blends show purer domains than the QxT counterpart, and QxO-annealed exhibits much larger domains than QxT-annealed. This correlates overall with the lower fullerenes miscibility in QxO, and identifies that the miscibility is a thermodynamic driving force during device fabrication that needs to be considered alongside materials interactions with the solvents and solvent vapor pressure when devising optimized processes. Significantly, this driving force even asserts its impact when the films are frozen into the highly non-equilibrium morphology of un-annealed, as-cast thin films.

Additive processing causes a bimodal log-normal distribution of domains, which probably originates from two or more competing or sequential phase separation mechanism, the details of which are outside the scope of the present study. QxO-DIO has larger composition fluctuations than QxT-DIO, whereas QxO-DIO has a less pronounced bimodal distribution. Interestingly, relative to annealing, DIO mitigates the materials specific impact on the characteristic length scale of the morphology. It causes smaller domains for QxO and larger domains for QxT relative to annealing. Nonetheless, a material specific effect of DIO as additive has been observed in the different spatial frequency distribution of the morphology as well as the composition fluctuations.

Overall, we find thermal annealing works better than additive processing. Although there might be several factors for this, we note that VLM shows quasi bicontinuous morphology for both QxO- and QxT-based blends. This indicates the phase separation mechanism might be spinodal decomposition. The bi-continous morphology created may be an additional reason why thermal annealing works better than additive processing in these two cases.

Overall, we note that neither thermal annealing nor additive processing creates an optimized device, as the respective device parameters V_{oc}, J_{sc}, and FF are not optimized at the same time. Thermal annealing causes domains that are either too large (QxO) or too impure (QxT). DIO causes domains that are too large and possibly too pure. Improved control of morphology and purity through modified processing or materials chemistry is required. More aggressive thermal annealing to create purer domain for QxT-annealed blend, less aggressive annealing for QxO to reduce domain size, and better controlling the amount or nature of additive to yield smaller domains of suitable purity for QxT-DIO and QxO-DIO, should be favorable for the final device performance based on these materials.

Furthermore, the morphological differences even in morphologies far from equilibrium are overall consistent with measurements of fullerene miscibility in the polymers. Hence, miscibility can be used to predict relative domain size and purity. Although such a relation would be expected from thermodynamic principles, it is an aspect that has not yet been generally considered when designing new materials for OPV devices. Similarly, the material specific interactions with processing additives such as DIO should also be considered alongside interactions with solvents,[61,62] even though a guiding frame-work for synthesis remains to be developed. The development of such a frame-work would additionally lead to more efficient device optimization processing protocols. Our results also illustrate that a range of sophisticated tools have to be used in order to investigate all the important physical parameters.

4 Experimental section

4.1 Samples

The synthesis method of QxO and QxT polymers is presented in the literature.[30] $PC_{71}BM$ are purchased from Nano-C. Blend films for devices, X-ray scattering and X-ray absorption were prepared using an identical procedure.

4.2 Devices fabrication

Devices were fabricated by spin-coating blend solutions on PEDOT:PSS -coated (~40 nm) indium-tin-oxide (ITO) glass substrates and then annealing in air at 120 °C for 20 min. Blend solutions of polymer : fullerene were prepared from 1,2-dicholorobenzene with a weight ratio 1 : 2 and polymer concentration is 10 g l^{-1}. The thickness of the active layer was controlled by changing the spin speed. The blend films were annealed at 120 °C for 10 min on a hotplate (temperature monitored by a surface thermometer) before transferring to a vacuum evaporator inside a nitrogen purified glove box. The additive DIO was used at a concentration of 3% without further thermal annealing of the cast samples. Finally, a 1 nm LiF layer and an 80 nm aluminum layer were subsequently evaporated through a shadow mask making devices with active areas of ~11 mm^2.

4.3 Devices characterization

Device measurements were conducted under purified nitrogen. A Keithley 2400 was used to source-measure current density *vs.* voltage (*J–V*) curves under AM 1.5 simulated illumination with 100 mW cm^{-2} intensity. The intensity was calibrated with an NREL certified Si reference solar cell.

4.4 Grazing incidence wide-angle X-ray scattering (GIWAXS)

GIWAXS experiment was performed at beamline 7.3.3 of Advanced Light Source (ALS).[63] Samples were prepared using identical blend solutions as those used in devices on a PSS pre-coated Si substrate. The 10 keV X-ray beam was incident at a grazing angle of 0.12°, which maximized the scattering intensity from the samples. The scattered intensity was detected with a Pilatus detector.

4.5 Resonant Soft X-ray Scattering (R-SoXS & P-SoXS)

R-SoXS transmission measurements were performed at beamline 11.0.1.2 at the ALS.[64] Samples for R-SoXS measurements were first prepared on a PSS modified Si substrate under the same conditions as those used for devices fabrication, and then transferred to a 1 mm × 1 mm, 100 nm thick Si3N4 membrane supported by a 5 mm × 5 mm, 200 μm thick Si frame (Norcada Inc.). 2-D scattering patterns were collected by an in-vacuum CCD camera (Princeton Instrument PI-MTE). The sample detector distance was calibrated from diffraction peaks of a triblock copolymer poly(isoprene-*b*-styrene-*b*-2-vinyl pyridine), which has a known spacing of 391 Å. The beam size at the sample is approximately 100 μm by 200 μm.

4.6 Scanning Transmission X-ray microscopy

STXM measurements were performed at beamline 5.3.2 at the ALS.[65] The TEM grid-supported films were mounted in the sample chamber, which was evacuated to 0.3 mbar and subsequently refilled with 1/3 atm of helium. The intensity of the focused X-ray beam transmitted through the film was recorded using a scintillator and photomultiplier tube and measured as a function of energy and position.

Acknowledgements

X-ray characterization and device measurements by NCSU supported by the Division of Materials Science and Engineering, Basic Energy Science, Office of Science, U.S. Department of Energy under Contract DE-FG02-98ER45737. X-ray data is acquired at the Advanced Light Source, which is supported by the Director, Office of Science, Office of Basic Energy Sciences, of the U.S. Department of Energy under Contract No. DE-AC02-05CH11231. Jianhui Hou would like to thank financial support from the Chinese Natural Science Foundation of China (51173189) and International S&T Cooperation Program of China (2011DFG63460) for the synthesis of the materials.

References

1 V. Shrotriya, *Nat. Photonics.*, 2009, **3**, 447–449.
2 G. Li, R. Zhu and Y. Yang, *Nat. Photonics*, 2012, **6**, 153–161.
3 G. Li, V. Shrotriya, J. Huang, Y. Yao, T. Moriarty, K. Emery and Y. Yang, *Nat. Mater.*, 2005, **4**, 864–868.
4 Z. He, C. Zhong, S. Su, M. Xu, H. Wu and Y. Cao, *Nat. Photonics*, 2012, **6**, 591–595.
5 L. Dou, J. You, J. Yang, C.-C. Chen, Y. He, S. Murase, T. Moriarty, K. Emery, G. Li and Y. Yang, *Nat. Photonics*, 2012, **6**, 180–185.
6 M. Wang, X. Hu, P. Liu, W. Li, X. Gong, F. Huang and Y. Cao, *J. Am. Chem. Soc.*, 2011, **133**, 9638–9641.
7 W. Ma, J. R. Tumbleston, M. Wang, E. Gann, F. Huang and H. Ade, *Adv. Energy Mater.*, 2013, DOI: 10.1002/aenm.201200912.
8 H. Zhou, L. Yang, A. C. Stuart, S. C. Price, S. Liu and W. You, *Angew. Chem., Int. Ed.*, 2011, **50**, 2995–2998.
9 L. Yang, J. R. Tumbleston, H. Zhou, H. Ade and W. You, *Energy Environ. Sci.*, 2013, **6**, 316–326.
10 A. Stuart, J. R. Tumbleston, H. Zhou, H. Ade, W. Li and W. You, *J. Am. Chem. Soc.*, 2013, **135**, 1806–1815.
11 S. C. Price, A. C. Stuart, L. Yang, H. Zhou and W. You, *J. Am. Chem. Soc.*, 2011, **133**, 4625–4631.
12 M. C. Scharber, M. Koppe, J. Gao, F. Cordella, M. A. Loi, P. Denk, M. Morana, H.-J. Egelhaaf, K. Forberich, G. Dennler, R. Gaudiana, D. Waller, Z. Zhu, X. Shi and C. J. Brabec, *Adv. Mater.*, 2010, **22**, 367–370.
13 L. Huo, L. Ye, Y. Wu, Z. Li, X. Guo, M. Zhang, S. Zhang and J. Hou, *Macromolecules*, 2012, **45**, 6923–6929.
14 L. Huo, S. Zhang, X. Guo, F. Xu, Y. Li and J. Hou, *Angew. Chem., Int. Ed.*, 2011, **50**, 9697–9702.
15 L. Huo, X. Guo, S. Zhang, Y. Li and J. Hou, *Macromolecules*, 2011, **44**, 4035–4037.
16 D. Qian, W. Ma, Z. Li, X. Guo, S. Zhang, L. Ye, H. Ade, Z. Tan and J. Hou, *J. Am. Chem. Soc.*, 2013, **135**, 8464–8467.
17 X. Guo, M. Zhang, J. Tan, S. Zhang, L. Huo, W. Hu, Y. Li and J. Hou, *Adv. Mater.*, 2012, **24**, 6536–6541.
18 W. Ma, J. Y. Kim, K. Lee and A. J. Heeger, *Macromol. Rapid Commun.*, 2007, **28**, 1776–1780.
19 W. Chen, T. Xu, F. He, W. Wang, C. Wang, J. Strzalka, Y. Liu, J. Wen, D. J. Miller, J. Chen, K. Hong, L. Yu and S. B. Darling, *Nano Lett.*, 2011, **11**, 3707–3713.

20 X. Guo, C. Cui, M. Zhang, L. Huo, Y. Huang, J. Hou and Y. Li, *Energy Environ. Sci.*, 2012, **5**, 7943–7949.
21 F. Liu, Y. Gu, C. Wang, W. Zhao, D. Chen, A. L. Briseno and T. P. Russell, *Adv. Mater.*, 2012, **24**, 3947–3951.
22 L. Ye, S. Zhang, W. Ma, B. Fan, X. Guo, Y. Huang, H. Ade and J. Hou, *Adv. Mater.*, 2012, **24**, 6335–6341.
23 G. Li, Y. Yao, H. Yang, V. Shrotriya, G. Yang and Y. Yang, *Adv. Funct. Mater.*, 2007, **17**, 1636–1644.
24 J. Peet, J. Y. Kim, N. E. Coates, W. L. Ma, D. Moses, a. J. Heeger and G. C. Bazan, *Nat. Mater.*, 2007, **6**, 497–500.
25 N. D. Treat, M. Brady, G. Smith, M. F. Toney, E. J. Kramer, C. J. Hawker and M. L. Chabinyc, *Adv. Energy Mater.*, 2011, **1**, 82–89.
26 B. Watts, W. J. Belcher, L. Thomsen, H. Ade and P. C. Dastoor, *Macromolecules*, 2009, **42**, 8392–8397.
27 B. A. Collins, E. Gann, L. Guignard, X. He, C. R. McNeill and H. Ade, *J. Phys. Chem. Lett.*, 2010, **1**, 3160–3166.
28 B. A. Collins, Z. Li, C. R. McNeill and H. Ade, *Macromolecules*, 2011, **44**, 9747–9751.
29 N. D. Treat, A. Varotto, C. J. Takacs, N. Batara, M. Al-hashimi, M. J. Heeney, A. J. Heeger, F. Wudl, C. J. Hawker and M. L. Chabinyc, *J. Am. Chem. Soc.*, 2012, **134**, 15869–15879.
30 R. Duan, L. Ye, X. Guo, Y. Huang, P. Wang, S. Zhang, J. Zhang, L. Huo and J. Hou, *Macromolecules*, 2012, **45**, 3032–3038.
31 D. Chen, F. Liu, C. Wang, A. Nakahara and T. P. Russell, *Nano Lett.*, 2011, **11**, 2071–2078.
32 H. Yan, B. A. Collins, E. Gann, C. Wang and H. Ade, *ACS Nano*, 2012, **6**, 677–688.
33 S. Swaraj, C. Wang, H. Yan, B. Watts, J. Lüning, C. R. McNeill and H. Ade, *Nano Lett.*, 2010, **10**, 2863–2869.
34 B. A. Collins, J. E. Cochran, H. Yan, E. Gann, C. Hub, R. Fink, C. Wang, T. Schuettfort, C. R. McNeill, M. L. Chabinyc and H. Ade, *Nat. Mater.*, 2012, **11**, 536–543.
35 B. A. Collins, Z. Li, J. R. Tumbleston, E. Gann, C. R. McNeill and H. Ade, *Adv. Energy Mater.*, 2013, **3**, 65–74.
36 B. A. Collins, J. R. Tumbleston and H. Ade, *J. Phys. Chem. Lett.*, 2011, **2**, 3135–3145.
37 X. He, B. A. Collins, B. Watts, H. Ade and C. R. McNeill, *Small*, 2012, **8**, 1920–1927.
38 J. A. Bartelt, Z. M. Beiley, E. T. Hoke, W. R. Mateker, J. D. Douglas, B. A. Collins, J. R. Tumbleston, K. R. Graham, A. Amassian, H. Ade, J. M. J. Frechet, M. F. Toney and M. D. McGehee, *Adv. Energy Mater.*, 2013, **3**, 364–374.
39 J. R. Tumbleston, A. C. Stuart, E. Gann, W. You and H. Ade, *Adv. Funct. Mater.*, 2013, DOI: 10.1002/adfm.201300093.
40 N. Shin, L. J. Richter, A. Herzing, R. J. Kline and D. M. DeLongchamp, *Adv. Energy Mater.*, 2013, DOI: 10.1002/aenm.201201027.
41 Y. Sun, G. C. Welch, W. L. Leong, C. J. Takacs, G. C. Bazan and A. J. Heeger, *Nat. Mater.*, 2012, **11**, 44–48.
42 Y. Gu, C. Wang and T. P. Russell, *Adv. Energy Mater.*, 2012, **2**, 683–690.
43 J. T. Rogers, K. Schmidt, M. F. Toney, E. J. Kramer and G. C. Bazan, *Adv. Mater.*, 2011, **23**, 2284–2288.
44 S. Shoaee, S. Subramaniyan, H. Xin, C. Keiderling, P. S. Tuladhar, F. Jamieson, S. A. Jenekhe and J. R. Durrant, *Adv. Funct. Mater.*, 2013, DOI: 10.1002/adfm.201203148.
45 F. C. Jamieson, E. B. Domingo, T. McCarthy-Ward, M. Heeney, N. Stingelin and J. R. Durrant, *Chem. Sci.*, 2012, **3**, 485.
46 B. P. Lyons, N. Clarke and C. Groves, *Energy Environ. Sci.*, 2012, **5**, 7657–7663.
47 F. Liu, Y. Gu, J. W. Jung, W. H. Jo and T. P. Russell, *J. Polym. Sci., Part B: Polym. Phys.*, 2012, **50**, 1018–1044.
48 M. T. Dang, L. Hirsch, G. Wantz and J. D. Wuest, *Chem. Rev.*, 2013, **113**, 3734–3765.
49 B. P. Rand, D. Cheyns, K. Vasseur, N. C. Giebink, S. Mothy, Y. Yi, V. Coropceanu, D. Beljonne, J. Cornil, J.-L. Brédas and J. Genoe, *Adv. Funct. Mater.*, 2012, **22**, 2987–2995.
50 T. Coffey, S. Urquhart and H. Ade, *J. Electron Spectrosc. Relat. Phenom.*, 2002, **122**, 65–78.
51 B. A. Collins and H. Ade, *J. Electron Spectrosc. Relat. Phenom.*, 2012, **185**, 119–128.
52 E. Verploegen, R. Mondal, C. J. Bettinger, S. Sok, M. F. Toney and Z. Bao, *Adv. Funct. Mater.*, 2010, **20**, 3519–3529.
53 C. R. McNeill, K. Asadi, B. Watts, P. W. M. Blom and D. M. De Leeuw, *Small*, 2010, **6**, 508–512.
54 D. T. W. Toolan, A. J. Parnell, P. D. Topham and J. R. Howse, *J. Mater. Chem. A*, 2013, **1**, 3587.
55 D. Chen, A. Nakahara, D. Wei, D. Nordlund and T. P. Russell, *Nano Lett.*, 2011, **11**, 561–567.
56 Y. Vaynzof, D. Kabra, L. Zhao, L. L. Chua, U. Steiner and R. H. Friend, *ACS Nano*, 2011, **5**, 329–336.
57 K. W. Chou, B. Yan, R. Li, E. Q. Li, K. Zhao, D. H. Anjum, S. Alvarez, R. Gassaway, A. Biocca, S. T. Thoroddsen, A. Hexemer and A. Amassian, *Adv. Mater.*, 2013, **25**, 1923–1929.
58 S. Bertho, W. D. Oosterbaan, V. Vrindts, J. D'Haen, T. J. Cleij, L. Lutsen, J. Manca and D. Vanderzande, *Org. Electron.*, 2009, **10**, 1248–1251.
59 N. M. Bedford, M. B. Dickerson, L. F. Drummy, H. Koerner, K. M. Singh, M. C. Vasudev, M. F. Durstock, R. R. Naik and A. J. Steckl, *Adv. Energy Mater.*, 2012, **2**, 1136–1144.
60 S. Albrecht, S. Janietz, W. Schindler, J. Frisch, J. Kurpiers, J. Kniepert, S. Inal, P. Pingel, K. Fostiropoulos, N. Koch and D. Neher, *J. Am. Chem. Soc.*, 2012, **134**, 14932–14944.
61 F. Machui, S. Abbott, D. Waller, M. Koppe and C. J. Brabec, *Macromol. Chem. Phys.*, 2011, **212**, 2159–2165.
62 B. Walker, A. Tamayo, D. T. Duong, X.-D. Dang, C. Kim, J. Granstrom and T.-Q. Nguyen, *Adv. Energy Mater.*, 2011, **1**, 221–229.
63 A. Hexemer, W. Bras, J. Glossinger, E. Schaible, E. Gann, R. Kirian, A. MacDowell, M. Church, B. Rude and H. Padmore, *J. Phys.: Conf. Ser.*, 2010, **247**, 012007.
64 E. Gann, A. T. Young, B. A. Collins, H. Yan, J. Nasiatka, H. A. Padmore, H. Ade, A. Hexemer and C. Wang, *Rev. Sci. Instrum.*, 2012, **83**, 045110.
65 A. L. D. Kilcoyne, T. Tyliszczak, W. F. Steele, S. Fakra, P. Hitchcock, K. Franck, E. Anderson, B. Harteneck, E. G. Rightor, G. E. Mitchell, A. P. Hitchcock, L. Yang, T. Warwick and H. Ade, *J. Synchrotron Radiat.*, 2003, **10**, 125–136.

